

Pyramid Sketch: a Sketch Framework for Frequency Estimation of Data Streams

Tong Yang^{1,2}, Yang Zhou¹, Hao Jin¹, Shigang Chen³, Xiaoming Li¹

¹Department of Computer Science and Technology, Peking University, China

²Collaborative Innovation Center of High Performance Computing, NUDT, Changsha, China

³Department of Computer & Information of Science & Engineering, University of Florida, USA

Email: yangtongemail@gmail.com, zhou.yang@pku.edu.cn,

jin.hao@pku.edu.cn, sgchen@cise.ufl.edu, lxm@pku.edu.cn

ABSTRACT

Sketch is a probabilistic data structure, and is used to store and query the frequency of any item in a given multiset. Due to its high memory efficiency, it has been applied to various fields in computer science, such as stream database, network traffic measurement, *etc.* The key metrics of sketches for data streams are accuracy, speed, and memory usage. Various sketches have been proposed, but they cannot achieve both high accuracy and high speed using limited memory, especially for skewed datasets. To address this issue, we propose a sketch framework, the Pyramid sketch, which can significantly improve accuracy as well as update and query speed. To verify the effectiveness and efficiency of our framework, we applied our framework to four typical sketches. Extensive experimental results show that the accuracy is improved up to 3.50 times, while the speed is improved up to 2.10 times. We have released our source codes at Github [1].

1. INTRODUCTION

1.1 Background and Motivation

Given a multiset, estimating the frequency of each item is a critical problem in data stream applications. A **multiset** refers to a set in which each item can appear multiple times. In scenarios such as real-time IP traffic, graph streams, web clicks and crawls, sensor database, and natural language processing (NLP) [2–6], the massive data are often organized as high-speed streams, requiring servers to record stream information in real time. Due to the high speed of data streams, it is often impractical to achieve accurate recording and estimating of item frequencies. Therefore, estimation of item frequencies by probabilistic data structures becomes popular and gains wide acceptances [7–9]. Sketches are initially designed for the estimation of item frequencies in data streams [10–15], and now have been applied

to many more fields, such as sparse approximation in compressed sensing [16], natural language processing [17, 18], data graph [19, 20], and more [21]. Note that we mainly *focus on the sketches used for frequency estimation in this paper.*

According to our analysis of real datasets and literatures [7, 9], the item frequencies in data streams are often highly skewed. In other words, most items are cold (*i.e.*, have a low frequency), while a few items are hot (*i.e.*, have a high frequency). For convenience, we use **hot items** and **cold items** to represent them in this paper. All existing sketches use counters to store frequencies, but it is difficult to find a proper size for the counters to fit these highly skewed data streams. For example, the frequencies of most items are cold (< 16), while the frequencies of a few hot items are larger than 40,000. Given the size of memory usage, 1) if each counter is 4 bits wide, the number of counters (\mathcal{C}) will be large, and the estimation of cold items will be very accurate. Unfortunately, hot items will incur overflows of counters, and this can hardly be acceptable in many applications. 2) If we allocate 16 bits to each counter, the number of counters will decrease to $\mathcal{C}/4$, and the accuracy of the sketch will drop drastically. What is worse, the frequency of the hottest item is **unknown** in many applications, which makes it hard to determine the counter size. Unfortunately, existing sketches (CM sketches [8], CU sketches [22], Count sketches [23], and Augmented sketches [7]) have to allocate enough bits for each counter, thus can hardly work well in real data streams that are highly skewed. The **design goal** of this paper is to *devise a framework which not only prevents counters from overflowing without the need of knowing the frequency of the hottest item in advance, but also can achieve high accuracy, high update speed, and high query speed at the same time.*

1.2 The Proposed Solution

In this paper, we propose a sketch framework, namely the Pyramid sketch, as it employs a pyramid-shaped data structure. The key idea of our Pyramid framework is *to automatically enlarge the size of the corresponding counters according to the current frequency of the incoming item, while achieving close to 1 memory access and 1 hash computation for each insertion.* Our proposed enlarging strategy uses geometric progression to guarantee that any practical large frequency can be represented within bounded memory usage. The pivotal technique is **counter-pair sharing**, which can significantly improve the accuracy.

*Shigang Chen is the corresponding author of this paper. This work is partially supported by National Basic Research Program of China (2014CB340400). This work is licensed under the Creative Commons Attribution-NonCommercial-NoDerivatives 4.0 International License. To view a copy of this license, visit <http://creativecommons.org/licenses/by-nc-nd/4.0/>. For any use beyond those covered by this license, obtain permission by emailing info@vlldb.org.

Proceedings of the VLDB Endowment, Vol. 10, No. 11
Copyright 2017 VLDB Endowment 2150-8097/17/07.

Considering the significance of insertion speed in high-speed data streams, we further propose another four techniques: 1) **word constraint**, 2) **word sharing**, 3) **one hashing**, and 4) **Ostrich policy**, to accelerate the insertion speed, while keeping the high accuracy.

To verify the universality of our sketch framework, we apply Pyramid to four typical sketches: CM sketches, CU sketches, Count sketches, and A sketches. In real data streams, we recommend using P_{CU} sketch which represents the CU sketch using Pyramid, as it achieves the highest accuracy and highest insertion speed at the same time.

2. RELATED WORK

The issue of estimation of the item frequency in a multiset is a fundamental problem in databases. The solutions can be divided into the following three categories: sketches, Bloom filter variants, and counter variants.

Sketches: Typical sketches include CM sketches [8], CU sketches [22], Count sketches [23], Augmented sketches [7], and more [24, 25]. A comprehensive survey about sketch algorithms is provided in the literature [9]. A CM sketch [8] consists of d arrays, $A_1 \dots A_d$, and each array consists of w counters. There are d hash functions, $h_1(\dots) \dots h_d(\dots)$ ($1 \leq h(\dots) \leq w$). When inserting an item e , the CM sketch increments all the **d mapped counters**¹ $A_1[h_1(e)] \dots A_d[h_d(e)]$ by 1. When querying an item e , the CM sketch reports the minimal one among the d mapped counters. The CU sketch [22] is similar to the CM sketch except that it only increments the smallest counter(s)² among the d mapped counters for each insertion. The Count sketch [23] is also similar to the CM sketch except that each array is associated with two hash functions. The Augmented sketch targets at improving accuracy by using one additional filter to dynamically capture hot items, suffering from complexities, slow update and query speed. The A sketch adds an additional filter (which is actually a queue with k items) to an existing sketch \mathcal{T} . The A sketch is very accurate only for those items in the filter. The authors focus on querying the hot items by using query sets sampled from the whole multiset. That is why their experimental results of the A sketch significantly outperform the CM sketch. Among these sketches, the CU sketch [22] achieves the highest accuracy when using the same amount of memory. Unfortunately, *all these sketches have three shortcomings for skewed datasets: 1) not accurate enough; 2) requiring multiple memory accesses and hash computations for each insertion; 3) requiring to know the approximate frequency of the hottest item in advance.*

Bloom filter variants: The second kind of solutions is based on Bloom filter [26]. A standard Bloom filter can tell whether an item belongs to a set or not, but *cannot* estimate its frequency. Counting Bloom filters (CBF) [27] can be used to estimate the frequency of items in a multiset. CBF is quite similar to the CM sketches, except that CBF uses only one array. Several improvements based on CBF have been proposed, such as the Spectral Bloom Filter (SBF) [28], the Dynamic Count Filter (DCF) [29] and the Shifting Bloom filter [30, 31], and they all can store frequencies of items.

Counter variants: Two typical algorithms are the counter braids [32] and Random Counters [2]. Counter braids can

¹For convenience, we call them **d mapped counters**.

²We use counter(s) because there may be multiple smallest counters.

report the frequencies of all items one time by post processing. It needs to know the IDs of all distinct items. The authors of Counter braids also admit that it cannot support instant point query [32]. The estimation method in Random Counters [2] is called CSM. It can achieve fast update speed at the cost of accuracy.

Summary: Although there are various algorithms for frequency estimation of multisets, no existing sketch can achieve high accuracy and one memory access per insertion, especially for skewed datasets.

3. PYRAMID SKETCH FRAMEWORK

In this section, we present two key techniques of our Pyramid framework: **counter-pair sharing** and **word acceleration**. Counter-pair sharing is used to *dynamically assign appropriate number of bits for different items with different frequencies*. Word acceleration can achieve one memory access and one hash computation per update, so as to significantly accelerate the update speed of sketches. We also present one further optimization method: Ostrich policy. Note that we introduce the techniques not in isolation, but one at a time on top of all previous techniques.

3.1 Technique I: Counter-pair Sharing

Data Structure: As shown in Figure 1, our Pyramid framework consists of λ layers, where we represent the i^{th} layer with L_i . L_i consists of w_i counters where $w_{i+1} = w_i/2$ ($1 \leq i \leq \lambda - 1$), and each counter contains δ bits. We represent the j^{th} counter of the i^{th} layer with $L_i[j]$. The first layer L_1 is associated with d independent hash functions $h_i(\dots)$ ($1 \leq i \leq d$), whose outputs are uniformly distributed in the range $[1, w_1]$. The i^{th} layer L_i is associated with the $i + 1^{th}$ layer L_{i+1} in the following way: two adjacent counters at L_i are associated with one counter at L_{i+1} . In other words, $L_i[2j - 1]$ and $L_i[2j]$ are associated with $L_{i+1}[j]$. $L_i[2j - 1]$ and $L_i[2j]$ are defined as the **sibling counters**. $L_{i+1}[j]$ is defined as the **parent counter** of $L_i[2j - 1]$ and $L_i[2j]$. $L_i[2j - 1]$ is defined as the **left child counter** of $L_{i+1}[j]$, and $L_i[2j]$ is defined as the **right child counter** of $L_{i+1}[j]$.

There are two types of counters: **pure counters** and **hybrid counters**. The first layer L_1 is composed of pure counters, while the other layers are composed of hybrid counters. The pure counter is only used for recording the frequencies. In other words, all the δ bits of the pure counters are used for counting, representing a range $[0, 2^\delta - 1]$. The hybrid counter with δ bits is split into three parts: *the left flag, the counting part, the right flag*. The **left flag** (1 bit) indicates whether its left child counter is overflowed, while the **right flag** (1 bit) indicates whether its right child counter is overflowed. The **counting part** ($\delta - 2$ bits) ranging from 0 to $2^{\delta-2} - 1$ is used for counting. For convenience, we use $L_i[j].lflag$, $L_i[j].count$, $L_i[j].rflag$ to represent the three parts of counter $L_i[j]$.

There are following three primary operations in our Pyramid framework: insertion, deletion, and query. Initially, all the counters at all the layers are 0.

Insertion: When inserting an item e , we first compute the d hash functions $h_1(e), h_2(e), \dots, h_d(e)$ ($1 \leq h(\dots) \leq w_1$) to locate the **d mapped counters** $L_1[h_1(e)], L_1[h_2(e)], \dots, L_1[h_d(e)]$ at layer L_1 . Different sketches will perform different incrementing operations on these d counters. During

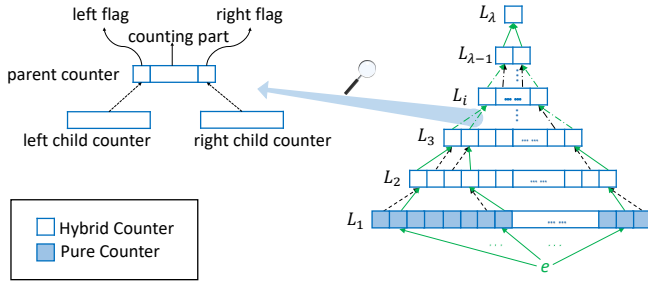


Figure 1: Counter-pair sharing technique.

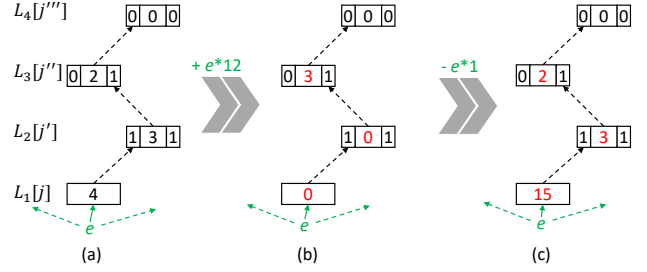
the incrementing process, if any of the d counters overflows, we simply record the overflow in the **parent counter**. This is called **carryin**.

The **carryin** operation is based on the following observation about practical datasets that are skewed: the number of overflowed counters is small, and in most cases at most one of the **sibling counters** overflows. Consider that $L_1[j]$ overflows. Let its parent counter be $L_2[j']$. Without loss of generality, assume $L_1[j]$ is the left child of $L_2[j']$. We check $L_2[j'].lflag$. If the flag is off, we turn it on and increment $L_2[j'].count$; if the flag is on, we only increment $L_2[j'].count$. If $L_2[j'].count$ does not overflow, insertion ends. Otherwise, we repeat the carryin operation at layer L_2 , and the operation will be performed layer by layer until there is no overflow. In this way, we dynamically assign an appropriate number of higher-order bits to record the incoming items, so as to minimize memory waste.

Example I: As shown in Figure 1 (a)(b), each pure counter consists of 4 bits, so does each hybrid counter. In each hybrid counter, the counting parts consist of 2 bits. As shown in the figure, the value of $L_1[j]$, the three parts of $L_2[j']$ and $L_3[j'']$ and $L_4[j''']$ are 4, $\langle 1, 3, 1 \rangle$, $\langle 0, 2, 1 \rangle$, $\langle 0, 0, 0 \rangle$, respectively. Suppose $L_1[j]$ is incremented by 12, $L_1[j]$ overflows, and the **carryin** operations are performed as follows.

- 1) $L_1[j]$ is set to 0;
- 2) $L_2[j'].lflag$ keeps on;
- 3) $L_2[j'].count$ is set to 0;
- 4) $L_3[j''].rflag$ keeps on;
- 5) $L_3[j''].count$ is incremented to 3.

Deletion: This framework supports deletions if and only if the sketch used in our framework supports deletions, such as the CM sketch [8], the Count sketch [23], the CSM sketch [2], etc. To delete an item e , we first check the d mapped counters $L_1[h_1(e)], L_1[h_2(e)], \dots, L_1[h_d(e)]$, and perform different deletion strategies according to the specific sketch. *The operation of decrementing a counter is exactly the reverse process of incrementing a counter.* Specifically, to decrement a pure counter $L_1[j]$, if it is non-zero, we just decrement it by 1. Otherwise, we set $L_1[j]$ to the maximum value $(2^\delta - 1)$, and then decrement its parent counter recursively. Without loss of generality, we only show the situation of only accessing or modifying *left flags*. To decrement a hybrid counter $L_i[j]$, $L_i[j].lflag$ must be on. There are the following three cases. 1) If $L_i[j].count$ is larger than 1, we just decrement it by 1. 2) If $L_i[j].count$ is 0, we just set it to $2^{\delta-2} - 1$, and then decrement its parent counter recursively. 3) If $L_i[j].count$ is 1, we first set it to 0, and turn $L_i[j].lflag$ off if the left flag of its parent counter is off.



Example III: As shown in Figure 1 (b)(c), the parameters of pure counter and hybrid counters are same as those of Example I. As shown in the figure, the value of $L_1[j]$, the three parts of $L_2[j']$ and $L_3[j'']$ and $L_4[j''']$ are 0, $\langle 0, 3, 1 \rangle$, $\langle 0, 0, 0 \rangle$, respectively. Suppose $L_1[j]$ is decremented by 1 and the deletion operations are performed as follows.

- 1) $L_1[j]$ is set to 15;
- 2) $L_2[j'].lflag$ keeps on, and $L_2[j'].count$ is set to 3;
- 3) $L_3[j''].rflag$ keeps on, and $L_3[j''].count$ is set to 2.

Algorithm 1: ReportVal(i, j_i).

```

/* assume that all the child counters are the
left child counters */
1 if  $i=1$  then
2   return  $L_1[j_1] + ReportVal(i + 1, j_{i+1})$ ;
3 if  $L_i[j_i].lflag == false$  then
4   return 0;
5 if  $L_i[j_i].lflag == true \ \&\& \ L_i[j_i].rflag == true$  then
6   return  $(L_i[j_i].count - 1) \times 2^{\delta+(i-2) \times (\delta-2)} +$ 
    $ReportVal(i + 1, j_{i+1})$ 
7 else
8   return
    $L_i[j_i].count \times 2^{\delta+(i-2) \times (\delta-2)} + ReportVal(i + 1, j_{i+1})$ 

```

Query: When querying an item e , we first compute d hash functions to find the d mapped counters $L_1[h_1(e)], L_1[h_2(e)], \dots, L_1[h_d(e)]$. These d mapped counters at layer L_1 share the same array of w_1 counters. Below we focus on describing the operations of querying the first mapped counter $L_1[j_1]$ ($j_1 = h_1(e)$), and the operations for other $d - 1$ counters are analogous. Let the parent counter and the ancestor counters of $L_1[j_1]$ be $L_2[j_2], L_3[j_3], \dots, L_\lambda[j_\lambda]$, respectively. Without loss of generality, we consider the case where $L_i[j_i]$ is the left child of $L_{i+1}[j_{i+1}]$, for $1 \leq i < \lambda$. According to Algorithm 1, we recursively assemble the counter value top-down, layer by layer, until the left flag is off. The result is a final **reported value** $ReportVal(1, j_1)$, also denoted as $\mathcal{R}(L_1[j_1])$ for convenience. In line 5 – 8, if the left flag and right flag of $L_i[j_i]$ are both on, its left child counter and right child counter must have both overflowed *at least once*. Therefore, we subtract 1 from $L_i[j_i].count$, so as to reduce the overestimation error incurred due to collision in counter-pair sharing. After obtaining the d reported value: $\mathcal{R}(L_1[h_1(e)]), \mathcal{R}(L_1[h_2(e)]), \dots, \mathcal{R}(L_1[h_d(e)])$, we produce the query output based on the specific sketch under

use. For example, for CM and CU, we simply report the minimum value of the d reported values.

Example III: As shown in Figure 1 (c), the parameters of pure counter and hybrid counters are same as those of Example I. As shown in the figure, the value of $L_1[j]$, the three parts of $L_2[j']$ and of $L_3[j'']$ and $L_4[j''']$ are 15, $\langle 1, 3, 1 \rangle$, $\langle 0, 2, 1 \rangle$, $\langle 0, 0, 0 \rangle$. The process of getting $\mathcal{R}(L_1[j])$ is shown as follows.

- 1) $L_1[j]$ is 15;
- 2) $L_2[j'].lflag$ is on and $L_2[j'].count$ is 3;
- 3) $L_3[j''].rflag$ is on and $L_3[j''].count$ is 2;
- 4) $L_4[j'''].lflag$ is off and the recursive operation ends;
- 5) The reported value is $15 + (3-1)*2^4 + (2-0)*2^6 = 175$.

3.2 Technique II: Word Acceleration

Word Constraint Technique: In the word constraint technique, we make two minor modifications: 1) we set the counter size δ to 4 bits; 2) we confine the d mapped counters at layer L_1 to a single machine word. In this way, the average number of memory accesses per insertion or query is significantly reduced. Let the size of a machine word be \mathcal{W} bits. Each machine word is comprised of $\mathcal{W}/4$ counters. Because there are w_1 counters at layer L_1 , that translates to $4w_1/\mathcal{W}$ machine words. Layer L_1 is associated with $d+1$ hash functions $h_i(\cdot)$ ($1 \leq i \leq d+1$). The first hash function is used to associate each item with a specific word Ω , and the remaining d hash functions are used to identify d mapped counters in the word Ω . Our word constraint technique is based on the following facts: 1) In our framework, each counter is small (e.g., 4 bits), while a machine word is usually 64 bits wide on many of today’s CPUs. 2) The size of a machine word can be much larger on GPU platforms. For example, one memory access can read up to 1024 bits in some commodity GPUs [33].

Therefore, one machine word on CPU or GPU can typically contain a reasonably large number of small counters used in our framework. Note that the actual operations of insertion, deletion and query stay the same under the word constraint.

Obviously, after using the word constraint technique, the average numbers of memory accesses per insertion, deletion or query are reduced to around $1/d$, as all the d mapped counters can be read/written within one memory access. Next, we derive an upper-bound of the average number of memory accesses for each insertion as follows. When inserting an item, suppose $\Pr(\text{layer } L_1 \text{ overflows}) < \rho$ and $\Pr(\text{layer } L_{i+1} \text{ overflows} \mid \text{layer } L_i \text{ overflows}) < \sigma$ (< 1) ($1 \leq i < \lambda$). The average number of memory accesses represented by \bar{t} is determined by the following formula.

$$\bar{t} < 1 + \sum_{k=0}^{\infty} \rho \sigma^k = 1 + \frac{\rho}{1 - \sigma} \quad (1)$$

In our experiments of IP traces, ρ is approximate to 0.05 and σ is approximate to 0.25. Therefore, the average number of memory accesses for each insertion \bar{t} is less than $1 + 0.05/(1 - 0.25) \approx 1.07$, which is consistent with our experimental results shown in Figure 19. Note that *one can simply improve the accuracy by confining the d mapped counters into two or more separated machine words.*

On top of the Pyramid sketch with only counter-pair sharing, adding the technique of word constraint helps reduce memory accesses per insertion or query, but incurs severe

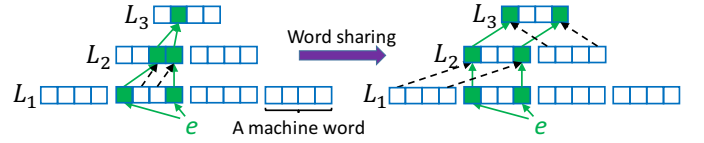


Figure 2: Example of word sharing technique.

accuracy loss in the meantime. The main reason for accuracy loss is that after implementing the **carryin** operation, the probability of collision among counters in the same machine word increases sharply at higher layers. More specifically, given an item e , its d counters at layer L_1 are mapped to one machine word, while the parent counters of these d counters are mapped to half of a word at layer L_2 . The ancestor counters are mapped to even small ranges in a word at higher layers, resulting in more collisions. To address this issue, we propose a new technique as follows.

Word Sharing Technique: The methodology of this technique is managing to make the parent counters and ancestor counters of the d mapped counters always fall in a constant range (*i.e.*, a machine word) instead of smaller and smaller ranges, so as to reduce collisions. Specifically, our word sharing technique works as follows: 1) Similar to the definition of parent counter, left child counter, right child counter, we have **left child word**, **right child word**, and **parent word**, where the left child word and the right child word are adjacent at layer L_i , sharing the same parent word at the next layer L_{i+1} . 2) The i^{th} counter in the left child word and the i^{th} counter in the right child word share the i^{th} counter in the parent word. In this way, the collisions in counter-pair sharing are alleviated, and the accuracy is significantly improved.

Example IV: In Figure 2, we set $\lambda = 3$, $d = 2$, and $w_1 = 16$. Each machine word consists of 4 counters. Without the word sharing technique, the d mapped counters at layer L_1 belong to a machine word, their parent counters belong to half of a machine word at layer L_2 , and their layer-3 ancestors belong to a quarter word, which is one counter in this example. In contrast, with the word sharing technique, the parent/ancestor counters of the d mapped counters always fall in a single machine word at each layer.

One Hashing Technique: More hash computations result in slower speeds for update and query. Ideally, only one hash computation is performed for each insertion, deletion or query. Towards this goal, we propose to use **one hashing** technique. The idea is to *split the value that a hash function produces into several segments, and each segment is used to locate a word or a counter, so as to reduce the hash computation.* A hash function usually produces a value of 32 or 64 bits. Given a hash function with 32-bit output, we may use the first 16 bits to locate a word in a Pyramid sketch. Suppose a word is 64 bits long. Locating one of the 16 counters in a word requires 4 hash bits. In total, we need 16 hash bits to locate 4 counters in this word. In this way, we can use only one hash computation to handle a Pyramid sketch which originally requires 4 hash computations with at most 2^{16} words at the layer L_1 . Similarly, we can use a hash functions with 64-bit output to support a Pyramid sketch ($d = 4$) with at most 2^{48} words, *i.e.*, 2048 TB memory at the layer L_1 , which should be large enough for all practical cases.

3.3 Further Optimization Method

Ostrich Policy: For sketches which need to know the reported values of the d mapped counters during each insertion (such as the CU sketch), multiple layers need to be accessed. To reduce the number of layer accesses, we propose a novel strategy, namely **Ostrich policy**. The key idea of **Ostrich policy** is ignoring the second and higher layers when getting the reported values of the d mapped counters. Here we take the CU sketch as an example. When inserting an item e , suppose the counter(s) with the *smallest value* among the d mapped counters is $L_1[j]$, we just increment the counter $L_1[j]$ by 1. Note that the *reported value* of $L_1[j]$ is not always the smallest among that of the d mapped counters. If there are multiple smallest ones, we perform the increment operation on all of them. Through the Ostrich policy, the insertion speed of our framework will be significantly improved.

One may argue that Ostrich policy could degrade the accuracy a lot. Actually, our experimental results show that Ostrich policy does help in improving the accuracy. Let us take the CU sketch as an example to explain this counter-intuitive phenomena. The CU sketch always increments the smallest counter(s) by 1 for each insertion. However, in many cases, the smallest counter(s) are already larger than their real frequency. In such cases, incrementing the smallest counter(s) is not the best strategy, while a new strategy of incrementing the smallest counter(s) with **high probability** often contributes to better accuracy. Ostrich policy is one efficient implementation of this new strategy.

3.4 Advantages over Prior Art

Compared to existing sketches, our Pyramid framework has the following advantages: 1) It is much more memory efficient because any an incoming item with different frequency are dynamically assigned appropriate number of bits. In other words, when using the same memory size, our framework can achieve a much higher accuracy. 2) It is much faster in terms of update and query speed, because it can read or write d mapped counters in one memory access, and only one hash computation is needed. 3) What is more, it also addresses another shortcoming of all existing sketches – word alignment. For example, given a multiset with a maximum frequency of 1000, the counter size in existing sketches should be 10 bits. As a result, some counters will traverse two bytes or two words, which will make the read or write operations of counters inefficient. In contrast, in our Pyramid framework, the word alignment can be perfectly achieved by setting the counter size δ to 4 bits.

4. MATHEMATICAL ANALYSES

In this section, we derive the correct rate and error bound when applying Pyramid framework to the CM sketch. We call the CM sketch after using this framework the P_{CM} sketch. Similarly, we have P_{CU} , P_C , P_A .

4.1 Proof of No Under-estimation Error

In this subsection, we prove that P_{CM} sketch has no under-estimation error. Under-estimation error means that *the querying value is smaller than the real frequency*. According to the implementation of Pyramid sketch framework, there will always be a layer where the overflow will not occur in practice. Through following steps, we will prove that if no

overflow occurs at layer L_n ($1 \leq n \leq \lambda$), the P_{CM} sketch has no under-estimation error.

Step 1: Suppose $n = 1$. According to the implementation of our framework, layer L_1 performs exactly the same as the CM sketch if no overflow occurs at Layer L_1 . Since the CM sketch has no under-estimation error [8], the P_{CM} sketch also has no under-estimation in this case.

Step 2: Suppose $n = k - 1$ ($k \geq 2$). The P_{CM} sketch has no under-estimation error.

Step 3: Suppose $n = k$. For one certain counter $L_{k-1}[j]$ at layer L_{k-1} , its actual value is determined by $L_{k-1}[j].count$, and the number of overflows which is recorded in the counting part of its parent counter $L_k[j']$. However, the sibling counter of $L_{k-1}[j]$ may also contribute to $L_k[j'].count$. Thus, the actual number of overflows of $L_{k-1}[j]$ is no larger than $L_k[j'].count$. In this way, if we recover the value of $L_{k-1}[j]$ according to the $L_k[j'].count$, the value we get will be no less than the actual value of $L_{k-1}[j]$ before the overflow. Assuming the counting part of counters at layer L_{k-1} to be large enough, the P_{CM} sketch will not overflow at layer L_{k-1} , with the counting part of $L_{k-1}[j]$ no less than the actual value. Therefore, in this case, the P_{CM} sketch has no under-estimation error.

According to the above three steps, it can be concluded that the P_{CM} sketch has no under-estimation error.

4.2 Correct Rate of the P_{CM} sketch

Given a multiset with N distinct items, we build a P_{CM} sketch. Let N_i^3 ($1 \leq i \leq \lambda$) denote the number of distinct items whose corresponding mapped d counters' carryin operations stop exactly at layer L_i . Without loss of generality, we simply assume that the d mapped counters' carryin operations all stop at the same layer.

Let P_i^{acc} denote the probability that one arbitrary counter corresponding with one arbitrary item stores the accurate value at layer L_i . P_i^{acc} equals to the probability that no collision happens in one certain counter at layer L_i :

$$\begin{aligned} P_i^{acc} &= \left(\frac{w_i - 1}{w_i} \right)^{(\Phi_i \times N - 1) \times d} \times \left(\frac{\mathcal{W}/\delta - 1}{\mathcal{W}/\delta} \right)^{d-1} \\ &= \left(1 - \frac{2^{i-1}}{w_1} \right)^{(\Phi_i \times N - 1) \times d} \times \left(1 - \frac{\delta}{\mathcal{W}} \right)^{d-1} \quad (1 \leq i \leq \lambda) \end{aligned} \quad (2)$$

where

$$\Phi_i = \begin{cases} \frac{\sum_{k=i}^{\lambda} N_k}{N} & (1 \leq i \leq \lambda) \\ 0 & (i = \lambda + 1) \end{cases} \quad (3)$$

and $\Phi_i - \Phi_{i+1} = N_i/N$ ($1 \leq i \leq \lambda$).

Let \mathcal{P} denote the expectation of the probability that one arbitrary counter at layer L_1 reports the accurate result. We calculate every portions of this probability layer by layer and report the average value using the weight of N_i :

$$\mathcal{P} = \frac{\sum_{k=1}^{\lambda} \left[N_k \times \prod_{l=1}^k P_l^{acc} \right]}{N} = \sum_{k=1}^{\lambda} \left[(\Phi_k - \Phi_{k+1}) \times \prod_{l=1}^k P_l^{acc} \right] \quad (4)$$

Let C_r denote the correct rate of the estimation for one arbitrary item. This item suffers from an over-estimation

³ N_i can be derived through the dataset's specific distribution or obtained by experiments.

error only in the condition that there are collisions in all the d mapped counters, thus we get:

$$C_r = 1 - (1 - \mathcal{P})^d \quad (5)$$

For the same multiset, we build a CM sketch comprised of d arrays: $A_1 \dots A_d$, each of which consists of w counters. Let \mathcal{P}' denote the expectation of the probability that one arbitrary counter at one arbitrary array A_i ($1 \leq i \leq d$) reports the accurate result. We have:

$$\mathcal{P}' = \left(1 - \frac{1}{w}\right)^{N-1} \quad (6)$$

Let C'_r denote the correct rate of the estimation for one arbitrary item in this CM sketch. Analogous to the derivation of the P_{CM} sketch, we get:

$$C'_r = 1 - \left(1 - \mathcal{P}'\right)^d \quad (7)$$

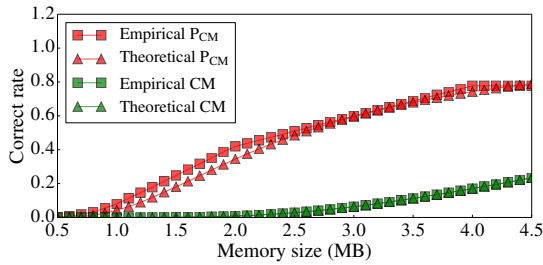


Figure 3: Comparison of empirical and theoretical correct rate with different memory sizes on one real IP trace.

Figure 3 plots the empirical and theoretical correct rates of the CM and P_{CM} sketch, on one real IP trace which will be mentioned in the Section 5.1. It shows that the theoretical results are consistent with the empirical results for both the CM and P_{CM} sketch. As the memory size becomes larger, the theoretical correct rates of the P_{CM} sketch get closer to the empirical result. This is because the randomness of hash values can be guaranteed with large enough mapping space. Besides, we observe that the P_{CM} sketch always significantly outperforms the CM sketch in terms of the correct rate empirically and theoretically.

4.3 Error Bound of the P_{CM} sketch

THEOREM 1. For an arbitrary item e_i , let \hat{f}_i denote its estimated frequency and f_i denote its real frequency. Let N denote the number of distinct items and V denote the sum of all items' real frequency, i.e., $V = \sum_{k=1}^N f_k$. The Φ_i is defined in Formula 3. Give a small variable ϵ , we have the following guarantee with probability at least $1 - \left(\frac{\Delta}{\epsilon}\right)^d$ (Δ is a constant relying on $N, \Phi_i, w_1, d, \mathcal{W}$ and δ):

$$\hat{f}_i \leq f_i + \epsilon \times V \quad (8)$$

PROOF. Every layers L_i ($2 \leq i \leq \lambda$) in the P_{CM} sketch can be considered to correspond with d virtual hash functions $h_1^i(\cdot), h_2^i(\cdot) \dots h_d^i(\cdot)$ ($1 \leq h(\cdot) \leq w_i$), which are determined by the initial d hash functions at the first layer L_1 and the carryin operation. Note that in this section, we call the initial d hash functions $h_1^1(\cdot), h_2^1(\cdot) \dots h_d^1(\cdot)$ ($1 \leq h(\cdot) \leq w_1$).

We define an indicator variable $I_{i,j,k,l}$, which is 1 if $h_j^l(e_i) = h_j^l(e_k)$, and 0 otherwise. Due to the independent hash functions, the expectation of this indicator variable can be derived as follows:

$$E(I_{i,j,k,l}) = \frac{1}{w_l} \times \frac{\Phi_l \times N \times d - d}{\Phi_l \times N \times d - 1} + \frac{1}{\mathcal{W}/\delta} \times \frac{d-1}{\Phi_l \times N \times d - 1} \quad (1 \leq l \leq \lambda)$$

For convenience, let E_l denote $E(I_{i,j,k,l})$, and let β_l denote $2^{\delta + (\delta-2) \times (l-2)}$. We define the variable $X_{i,j}$ as follows:

$$\begin{aligned} X_{i,j} &= (\Phi_1 - \Phi_2) \times \sum_{k=1}^N (f_k \times I_{i,j,k,1}) + \\ &= \sum_{l=2}^{\lambda} \left[(\Phi_l - \Phi_{l+1}) \times \sum_{k=1}^N \left(\frac{f_k}{\beta_l} \times I_{i,j,k,l} \times \beta_l \right) \right] \\ &= \sum_{l=1}^{\lambda} \left[(\Phi_l - \Phi_{l+1}) \times \sum_{k=1}^N (f_k \times I_{i,j,k,l}) \right] \end{aligned}$$

Obviously, it can be guaranteed that $X_{i,j}$ is a non-negative variable. $X_{i,j}$ reflects the expectation of the error caused by the collisions happening at all the layers when querying one arbitrary counter at layer L_1 . In other words, we have:

$$\mathcal{R}(L_1[h_j^1(e_i)]) = f_i + X_{i,j} \quad (9)$$

The expectation of $X_{i,j}$ is calculated as follows.

$$\begin{aligned} E(X_{i,j}) &= E \left\{ \sum_{l=1}^{\lambda} \left[(\Phi_l - \Phi_{l+1}) \times \sum_{k=1}^N (f_k \times I_{i,j,k,l}) \right] \right\} \\ &= \sum_{l=1}^{\lambda} \left[(\Phi_l - \Phi_{l+1}) \times \sum_{k=1}^N (f_k \times E(I_{i,j,k,l})) \right] \\ &= \sum_{l=1}^{\lambda} \left[(\Phi_l - \Phi_{l+1}) \times E_l \times \sum_{k=1}^N f_k \right] \\ &= \sum_{l=1}^{\lambda} [(\Phi_l - \Phi_{l+1}) \times E_l \times V] \\ &= V \times \sum_{l=1}^{\lambda} [(\Phi_l - \Phi_{l+1}) \times E_l] \\ &= V \times \Delta \end{aligned}$$

Where Δ denotes $\sum_{l=1}^{\lambda} [(\Phi_l - \Phi_{l+1}) \times E_l]$. Thus, we get:

$$V = \frac{E(X_{i,j})}{\Delta} \quad (10)$$

Then, by the Markov inequality, we get:

$$\begin{aligned}
& Pr \left[\hat{f}_i \geq f_i + \epsilon \times V \right] \\
&= Pr \left[\forall_j. \mathcal{R}(L_1[h_j^1(e_i)]) \geq f_i + \epsilon \times V \right] \\
&= Pr \left[\forall_j. f_i + X_{i,j} \geq f_i + \epsilon \times V \right] \\
&= Pr \left[\forall_j. X_{i,j} \geq \epsilon \times V \right] \\
&= Pr \left[\forall_j. X_{i,j} \geq \epsilon \times \frac{E(X_{i,j})}{\Delta} \right] \\
&= Pr \left[\forall_j. \frac{X_{i,j}}{E(X_{i,j})} \geq \frac{\epsilon}{\Delta} \right] \\
&\leq \left\{ E \left[\frac{X_{i,j}}{E(X_{i,j})} \right] / \frac{\epsilon}{\Delta} \right\}^d \\
&= \left(\frac{\Delta}{\epsilon} \right)^d
\end{aligned} \tag{11}$$

□

Using the same notations employed in the Theorem 1, we transform the error bound of the CM sketch given by the literature [8] into the following form:

THEOREM 2. *Give a small variable ϵ , we have the following guarantee with probability at least $1 - \left(\frac{1/w}{\epsilon}\right)^d$ (w is the number of counters of each array in the CM sketch):*

$$\hat{f}_i \leq f_i + \epsilon \times V \tag{12}$$

Figure 4 plots the empirical and theoretical guaranteed probabilities of the CM and P_{CM} sketch, on the synthetic dataset with skewness of 0.0 which will be mentioned in the Section 5.1. It shows the error bound of P_{CM} sketch is much better than that of the CM sketch. We use the synthetic dataset with skewness of 0.0 to evaluate the worst case performance (see Figure 9 and 10) of sketches, verifying the bounds of CM and P_{CM} . Note that in Figure 9 and 10, the AAE equals to the average $\hat{f}_i - f_i$ of all distinct items.

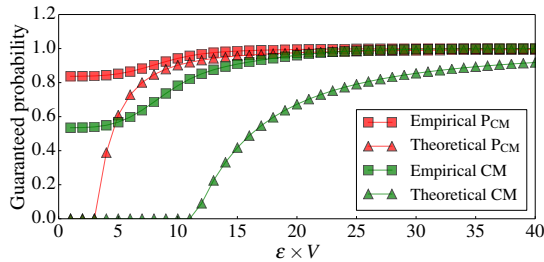


Figure 4: Comparison of empirical and theoretical error bound on one synthetic dataset with skewness 0.0.

5. PERFORMANCE EVALUATION

5.1 Experimental Setup

Datasets: We use three kinds of datasets as follows.

1) Real IP-Trace Streams: We obtain the real IP traces from the main gateway at our campus. The IP traces consist of flows, and each flow is identified by its five-tuple: source IP address, destination IP address, source port, destination port, and protocol type. The estimation of item

frequency corresponds to the estimation of number of packets in a flow. We divide 10M*10 packets into 10 datasets, and build a sketch with 1MB memory for each dataset. Each dataset includes around 1M flows. The flow characteristics in these datasets are similar. Take the first dataset as an example. The flow size ranges from 1 to 25,429 with a mean of 9.27 and a variance of 11,361. *Note that 41.8% flows only have one packet.* The length of items in each experimental dataset is 22 ~ 46 bytes.

2) Real-Life Transactional Dataset: We downloaded this dataset from the website [34]. This dataset is built from a spidered collection of web html documents. It generates from each document a distinct transaction containing the set of all the distinct terms (items) appearing within the document itself. Since this raw dataset is very large, we use the first 16M items and estimate the frequency of each distinct items. For this transactional dataset with 16M items, it contains 598,688 distinct items. The frequency ranges from 1 to 75,457, with a mean of 29.29 and a variance of 202,826.

3) Synthetic Datasets: We generate 11 stream datasets following the Zipf [35] distribution with the fixed total frequency of items (10M) but different skewnesses (from 0.0 to 1.0 with a step of 0.1) and different numbers of distinct items. The larger the skewness is, the more skewed this dataset is. The main part of our generator’s source codes come from a performance testing tool named Web Polygraph [36]. The maximum frequency of items in each dataset is 28 ~ 21423. The length of items in each dataset is all 13 bytes.

Implementation: We have implemented the sketches of CM [8], CU [22], C [23] and A [7] in C++. We apply our Pyramid framework to these sketches, and the results are denoted as P_{CM} , P_{CU} , P_C , and P_A . For P_{CM} , P_C and P_A , we apply the proposed techniques of counter-pair sharing and word acceleration (including word constraint, word sharing, and one hashing). For the P_{CU} sketch, we additionally apply the Ostrich policy, which is only suitable for CU. The hash functions used in the sketches are implemented from the 32-bit or 64-bit Bob Hash (obtained from the open source website [37]) with different initial seeds. For the sketches of CM and CU, we set the number of arrays to 4 and use 4 32-bit Bob Hashes. For the C sketch, we set the number of arrays to 4 and use 8 32-bit Bob Hashes⁴. For the A sketch, we set its filter size to 32 items as the original paper [7] recommends. For the CM sketch contained in the A sketch, we set the number of arrays to 4 and use 4 32-bit Bob Hashes. For all the above four sketches, we set the counter size to 16 bits in the experiments with the IP traces and synthetic datasets, and to 24 bits in the experiments with the transactional dataset, so as to accommodate the maximal frequency of items. For the sketches of P_{CM} , P_{CU} , P_C and P_A , we set the number d of mapped counters to 4, the counter size δ to 4 bits, and the machine word size \mathcal{W} to 64 bits. For each of these Pyramid sketches, we use 1 64-bit Bob hashes. In all our experiments with different sketches, we allocate the same amount of memory, 1 MB, by default unless specified otherwise. We allow the A sketch to use a small amount of additional memory for its filter, which is ≈ 0.4 KB and negligible when comparing with the total memory. Hence, the real memory allocation for A is 1MB +

⁴As mentioned before, in C, each array is associated with 2 hash functions.

0.4KB. The number of counters in each experiment can be easily calculated through the allocated memory size and the counter size in the sketch under use. All the implementation source code is made available at Github [1].

Computation Platform: We performed all the experiments on a machine with 12-core CPUs (24 threads, Intel Xeon CPU E5-2620 @2 GHz) and 62 GB total DRAM memory. CPU has three levels of cache memory: two 32KB L1 caches (one is a data cache and the other is an instruction cache) for each core, one 256KB L2 cache for each core, and one 15MB L3 cache shared by all cores.

5.2 Metrics

Average Absolute Error (AAE): AAE is defined as $\frac{1}{|\Psi|} \sum_{e_i \in \Psi} |f_i - \hat{f}_i|$, where f_i is the real frequency of item e_i , \hat{f}_i is the estimated frequency, and the Ψ is the query set. For the query set, the authors of the A sketch [7] use a sampled set of the whole multiset, mainly focusing on querying the hot items. Without knowing the details of the sampling method used by the A sketch paper [7], *we focus on the whole dataset by querying each distinct item only once*. That is the reason why the A sketch is only a little better than the CM sketch in terms of accuracy in the following experiments. To guarantee that our experiments are conducted head-to-head, we have released the related source codes and datasets at Github [1].

Average Relative Error (ARE): ARE is defined as $\frac{1}{|\Psi|} \sum_{e_i \in \Psi} |f_i - \hat{f}_i| / f_i$, where the meaning of each notation is the same as that in AAE. We explain the reason why AAE and ARE are sometimes larger than anticipated in the experiments. When a sketch uses compact memory (*e.g.*, 1 MB) to process massive data streams (*e.g.*, 10M items), significant over-estimations of cold items will become common [38]. Take the real IP traces for example. About 41.8% flows in these data streams only have one packet, while large flows have more than 10,000 packets. When a flow with one packet is estimated as 101, the absolute and relative errors will be both 100. This will make AAE and ARE much larger than anticipated.

The Average Number of Memory Accesses: The number of memory access is critical when implementing sketches on hardware, such as FPGA and ASIC. Therefore, we measure the average number of memory access of insertion, deletion and query for all sketches.

Throughput: We perform the insertion and query operations on CPU platform and calculate the throughput using mega-instructions per second (Mips). All the experiments are repeated 100 times to minimize accidental deviations.

5.3 Effects of Different Techniques

We have proposed five techniques: counter-pair sharing (T_1), word constraint (T_2), word sharing (T_3), one hashing (T_4), and Ostrich policy (T_5). We use $P_{CU}^{1 \sim i}$ ($1 \leq i \leq 5$) to denote the P_{CU} sketch with the first i techniques: T_1, T_2, \dots, T_i . Similar notations are introduced for other sketches as $P_{CM}^{1 \sim i}$, $P_C^{1 \sim i}$, and $P_A^{1 \sim i}$ ($1 \leq i \leq 4$); note that Ostrich policy does not apply to these sketches. In later subsections, we will abbreviate $P_{CM}^{1 \sim 4}$ to P_{CM} , $P_{CU}^{1 \sim 5}$ to P_{CU} , $P_C^{1 \sim 4}$ to P_C , and $P_A^{1 \sim 4}$ to P_A .

The experimental performance of the CU sketch in terms of accuracy and speed under the five techniques are shown in Figure 5, 6 and 7. We have the following five observations:

- 1) The counter-pair sharing technique (T_1) significantly reduces AAE and ARE, and slightly degrades the speeds of both insertion and query.
- 2) The word constraint technique (T_2) significantly reduces memory accesses per insertion or query, slightly lowers the throughput of both insertion and query, and incurs severe accuracy loss. Lower throughput is caused by extra hash computation for locating a machine word.
- 3) The word sharing technique (T_3) overcomes the main shortcoming of the word constraint, improving the accuracy without impact on the insertion and query speeds.
- 4) The one hashing technique (T_4) improves the speeds of insertion and query, while not affecting the accuracy.
- 5) The Ostrich policy technique (T_5) significantly improves the insertion speed, slightly improve the accuracy, and does not affect the query speed. Note that without using Ostrich policy, $P_{CU}^{1 \sim i}$ ($1 \leq i \leq 4$) always have to access multiple layers to know the reported values of the d mapped counters during each insertion. Therefore, $P_{CU}^{1 \sim i}$ ($1 \leq i \leq 4$) need more memory accesses per query than the final version $P_{CU}^{1 \sim 5}$.

5.4 Accuracy

We apply the Pyramid framework to four typical sketches: the CM, CU, C, and A sketch, and find that P_{CU} achieves the highest accuracy. Therefore, we recommend using the P_{CU} sketch in the application of data streams, and in most experiments, we compare the P_{CU} sketch with the above typical sketches. Note that in each of the parameter settings, the proposed Pyramid framework always improves the accuracies of CM, CU, C, and A. The positive impact of using Pyramid is demonstrated in Figure 8 and 12. In this section, we mainly use the P_{CU} sketch as an example to show the benefits of our Pyramid framework under varied parameter settings.

5.4.1 AAE (Average Absolute Error)

Our experimental results show that the AAEs of the CM, CU, C, and A sketch are 3.01, 2.02, 1.26 and 3.14 times higher than the AAEs of these sketches using our framework. Figure 8 plots the AAEs of different sketches on the transactional dataset. Since the C sketch needs to record the negative numbers during updates, we use one fifth of total memory to serve as the positive or negative markers. Those markers are accessed only when overflows happen during updates. For the C sketch, when we still confine the d mapped counters within only one machine word, the P_C sketch improves the accuracy only a little because of word constraint. To make a better trade-off, we confine the d mapped counters within two separated machine words, compensating for the accuracy loss caused by word acceleration. Note that for the P_{CM} , P_{CU} , and P_A sketch, *we still use one word constraint.*

Our experimental results show that on different IP traces, the AAEs of the CM, CU, C, and A sketch are 4.74, 2.50, 2.89 and 4.73 times higher than the AAE of the P_{CU} sketch. Figure 9 plots the AAEs of different sketches on different IP traces. The reason why the A sketch has the similar accuracy to the CM sketch is explained in Section 5.2.

Our experimental results show that on skewed datasets, the AAEs of the CM, CU, C, and A sketch are 4.75, 2.31, 3.67 and 4.75 times higher than the AAE of the P_{CU} sketch. Figure 10 plots the AAEs of different sketches on different datasets with the skewness increasing from 0.0 to 1.0 with a step of 0.1.

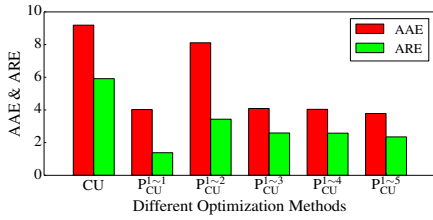


Figure 5: Comparison of AAE & ARE with different optimization methods on one real IP trace.

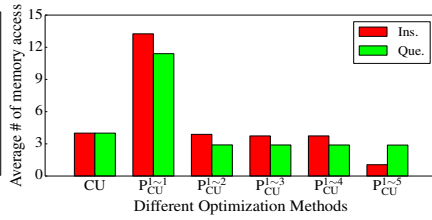


Figure 6: Comparison of average # memory accesses with different optimization methods on one real IP trace.

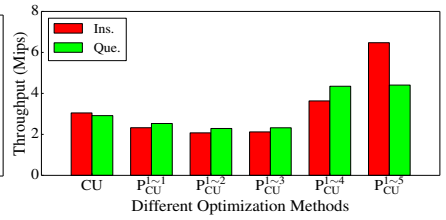


Figure 7: Comparison of throughput with different optimization methods on one real IP trace.

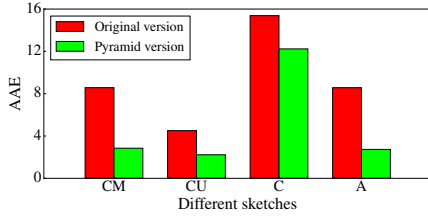


Figure 8: AAE comparison on the transactional dataset.

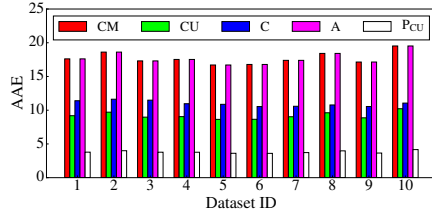


Figure 9: AAE comparison on different real IP traces.

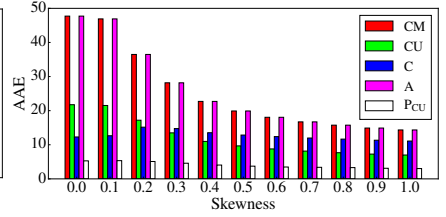


Figure 10: AAE comparison on synthetic datasets with different skewnesses.

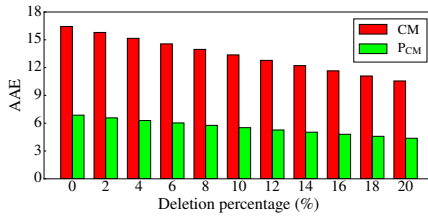


Figure 11: AAE comparison during deletions on one real IP trace.

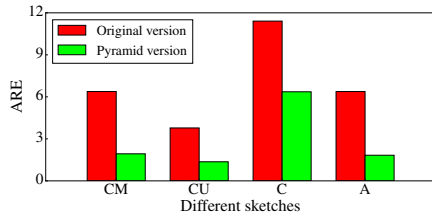


Figure 12: ARE comparison on the transactional dataset.

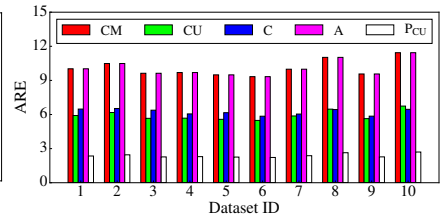


Figure 13: ARE comparison on different real IP traces.

Our experimental results show that during the process we delete items up to 20%, the AAE of the CM sketch is 2.39 times higher than the AAE of the P_{CM} sketch. Figure 11 plots the AAEs of the CM and P_{CM} sketch at a deletion percentage increasing from 0 to 20 by 2. We first insert 10 MB items into each sketch, then delete a specific percentage of items and calculate the AAEs of those distinct items with nonzero real frequency after each deletion.

5.4.2 ARE (Average Relative Error)

Our experimental results show that the AREs of the CM, CU, C, and A sketch are 3.31, 2.78, 1.79 and 3.50 times higher than the AREs of these sketches using our framework. Figure 12 plots the AREs of different sketches on the transactional dataset.

Our experimental results show that on different IP traces, the AREs of the CM, CU, C, and A are 4.24, 2.50, 2.42 and 4.24 times higher than the ARE of the P_{CU} sketch. Figure 13 plots the AREs of different sketches on different IP traces.

Our experimental results show that on skewed datasets, the AREs of the CM, CU, C, and A sketch are 5.02, 2.83, 3.26 and 5.02 times higher than the ARE of the P_{CU} sketch. Figure 14 plots the AREs of different sketches on different datasets with the skewness increasing from 0.0 to 1.0 by a step of 0.1.

Our experimental results show that during the process we delete items up to 20%, the ARE of the CM sketch is 2.48 times higher than the ARE of the P_{CM} sketch. Figure 15 plots the AREs of the CM and P_{CM} sketch at a deletion percentage increasing from 0 to 20 by 2.

5.4.3 Experiments on Memory Size and Word Size

As mentioned above, P_{CU} achieves the best accuracy, therefore, we mainly compare P_{CU} with the four typical sketches by varying the memory size or word size.

Our experimental results show that on different memory sizes, the AAEs of the CM, CU, C, and A sketch are 4.52, 2.43, 2.31 and 4.52 times higher than the AAE of the P_{CU} sketch. Figure 16 plots the AAEs of different sketches on different memory sizes increasing from 0.50MB to 2.00MB with a step of 0.25MB.

Our experimental results show that on different memory sizes, the AREs of the CM, CU, C, and A sketch are 4.28, 2.48, 2.19 and 4.28 times higher than the ARE of the P_{CU} sketch. Figure 17 plots the AREs of different sketches on different memory sizes increasing from 0.50MB to 2.00MB with a step of 0.25MB.

Our experimental results show that as the word size increases from 64 bits to 1024 bits, the AAE of the P_{CU} sketch decreases from 3.72 to 2.60 and the ARE of the P_{CU} sketch

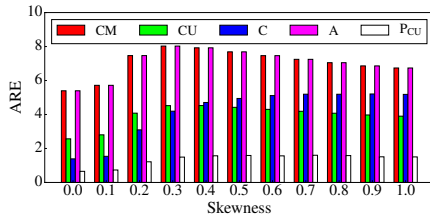


Figure 14: ARE comparison on synthetic datasets with different skewnesses.

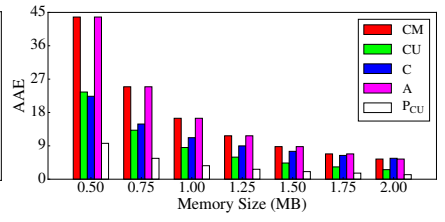
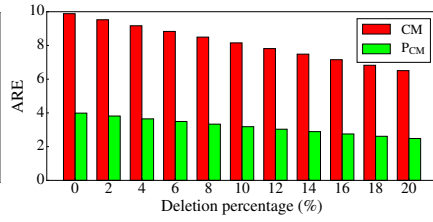


Figure 16: AAE comparison with different memory sizes on one real IP trace.

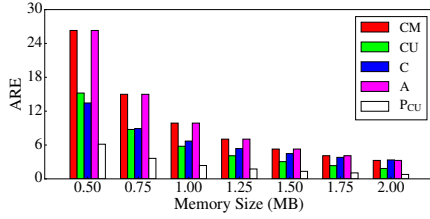


Figure 17: ARE comparison with different memory sizes on one real IP trace.

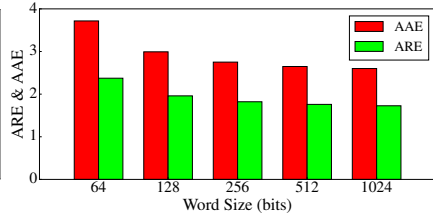


Figure 18: AAE & ARE of P_{CU} with different word sizes on one real IP trace.

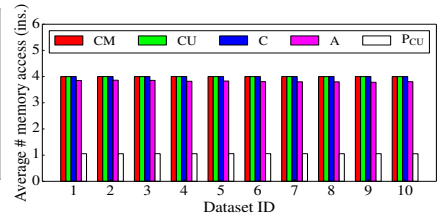


Figure 19: Comparison of average # memory accesses for each insertion on different real IP traces.

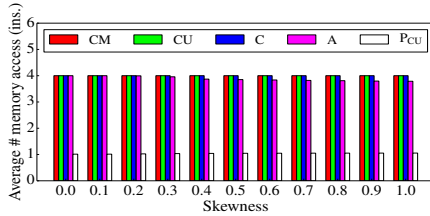


Figure 20: Comparison of average # memory accesses for each insertion on synthetic datasets with different skewnesses.

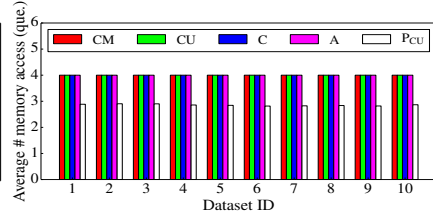


Figure 21: Comparison of average # memory accesses for each query on different real IP traces.

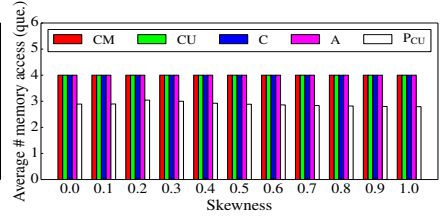


Figure 22: Comparison of average # memory accesses for each query on synthetic datasets with different skewnesses.

decreases from 2.37 to 1.73. Figure 18 plots the AREs and AAEs of the P_{CU} sketch on different word sizes multiplying from 64 bits to 1024 bits by 2.

5.5 Speed

We have conducted extensive experiments on speed of the CM, CU, C, and A sketch, and results show that after using the Pyramid framework, the update and query speed of all the sketches are significantly improved. Note that in each of the parameter settings, the Pyramid framework always improves the speeds of CM, CU, C, and A. In this section, we only present the results of P_{CU} .

5.5.1 The Average Number of Memory Access

In this section, when conducting the statistics for the A sketch, we do not include its number of memory access caused by searching in its filter, while searching the filter probably takes more time than querying the sketch part.

Insertion: Our experimental results show that the CM, CU, C, A and P_{CU} sketch need about 4, 4, 4, 3.80 and 1.05 average memory accesses for insertion, respectively. Figure 19 plots average numbers of memory access of different sketches on different real IP traces during insertions. For

the P_{CU} sketch, the average number is quartered from that of the other sketches by the word constraint method.

Our experimental results show that average numbers of memory access of the CM, CU, C sketch for each insertion keep unchanged (equal to 4), while that of the A sketch is 4.00 ~ 3.79 (with a mean of 3.90) and that of the P_{CU} sketch is 1.01 ~ 1.06 (with a mean of 1.04). Figure 20 plots average numbers of memory access of different sketches for each insertion on the synthetic datasets with different skewnesses.

Query: Our experimental results show that the CM, CU, C, A and P_{CU} sketch need about in average 4, 4, 4, 4.00 and 2.85 memory accesses for each query, respectively. Figure 21 plots average numbers of memory access of different sketches for each query on different real IP traces. We observe that the average number of memory access of the P_{CU} sketch for each query exceeds 2, owing to the corresponding flags check at the second layer L_2 for each query.

Our experimental results show that the average numbers of memory access of the CM, CU, C sketch for each query keep unchanged (equal to 4), while that of the A sketch is about 4.00 and that of the P_{CU} sketch is 2.89 ~ 2.79 (with a mean of 2.84). Figure 22 plots average numbers of memory access of different sketches for each query on the synthetic datasets

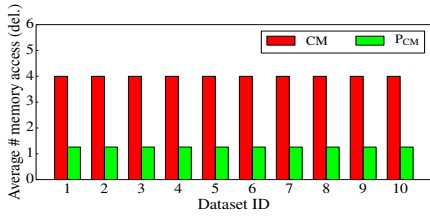


Figure 23: Comparison of average # memory accesses for each deletion on different real IP traces.

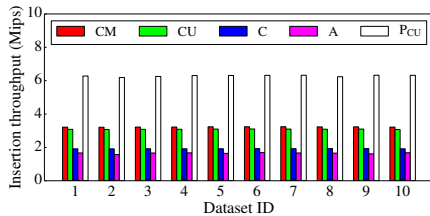


Figure 24: Comparison of insertion throughput on different real IP traces.

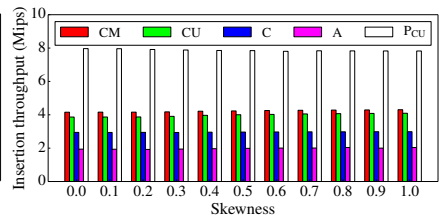


Figure 25: Comparison of insertion throughput on synthetic datasets with different skewnesses.

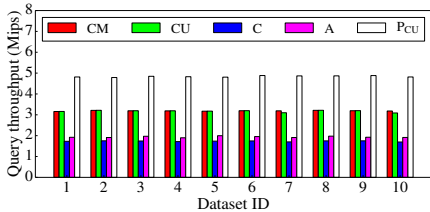


Figure 26: Comparison of query throughput on different real IP traces.

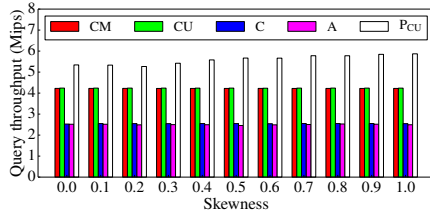


Figure 27: Comparison of query throughput on synthetic datasets with different skewnesses.

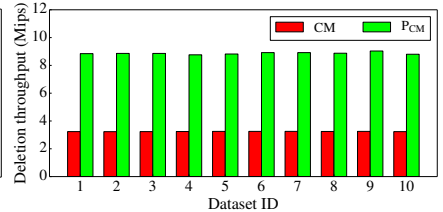


Figure 28: Comparison of deletion throughput on different real IP traces.

with different skewnesses. We observe that the P_{CU} sketch performs better on more skewed datasets for query.

Deletion: Our experimental results show that the CM and P_{CM} sketch need about in average 4 and 1.26 memory accesses for each deletion, respectively. Figure 23 plots average numbers of memory access of different sketches for each deletion on different IP traces. For the CU sketch, it does not support deletion. For the C and A sketch, their average numbers of memory access for each deletion are similar to that of the CM sketch because they have almost the same structure. We observe that the P_{CM} sketch considerably outperforms the CM sketch for deletion.

5.5.2 Throughput

Insertion: Our experimental results show that the insertion throughput of the P_{CU} sketch is about 1.97, 2.10, 3.32 and 3.82 times higher than those of the CM , CU , C and A sketch. Figure 24 plots the insertion throughput of different sketches on different real IP traces. We observe that the P_{CU} sketch always outperforms the other sketches, and at least twice insertion speed.

Our experimental results show that the insertion throughput of the P_{CU} sketch is about 1.83, 1.98, 2.61 and 3.85 times higher than those of the CM , CU , C and A sketch on the datasets with different skewnesses during insertions. Figure 25 plots the insertion throughput of different sketches on synthetic datasets with different skewnesses.

Query: Our experimental results show that the query throughput of the P_{CU} sketch is about 1.50, 1.50, 2.82 and 2.51 times higher than those of the CM , CU , C and A sketch. Figure 26 plots the query throughput of different sketches on different real IP traces.

Our experimental results show that the query throughput of the P_{CU} sketch is about 1.33, 1.33, 2.24 and 2.25 times higher than those of the CM , CU , C and A sketch on the datasets with different skewnesses. Figure 27 plots the query

throughput of different sketches on synthetic datasets with different skewnesses.

Deletion: Our experimental results show that the deletion throughput of the P_{CM} sketch is about 2.73 times higher than that of the CM sketch. Figure 28 plots the deletion throughput of different sketches on different real IP traces. We observe that the P_{CM} sketch considerably outperforms the CM sketch for deletion.

6. CONCLUSION

Sketches have been applied to various fields. In this paper, we propose a sketch framework - the Pyramid sketch, to significantly improve the update speed and accuracy. We applied our framework to four typical sketches: the CM , CU , Count, and Augmented sketch. Experimental results show that our framework significantly improves both accuracy and speed. We believe our framework can be applied to many more sketches. All related source codes are released at Github [1].

ACKNOWLEDGEMENTS

We would like to thank the anonymous reviewers for their thoughtful suggestions. This work is partially supported by Primary Research & Development Plan of China (2016YFB1000304), NSFC (61472009, 61672061), NSF (STC-1562485), SHENZHEN Research Project JCYJ20160330095313861, the Open Project Funding of CAS Key Lab of Network Data Science and Technology, Institute of Computing Technology, Chinese Academy of Sciences, and Special Fund for strategic pilot technology Chinese Academy of Sciences (XDA06010302).

7. REFERENCES

- [1] Source codes of Pyramid sketch and related sketches. https://github.com/zhouyangpkuer/Pyramid_Sketch_Framework.
- [2] Tao Li, Shigang Chen, and Yibei Ling. Per-flow traffic measurement through randomized counter sharing. *IEEE/ACM Transactions on Networking*, 20(5):1622–1634, 2012.
- [3] George Kollios, John W Byers, and et al. Robust aggregation in sensor networks. *IEEE Data Eng. Bull.*, 28(1):26–32, 2005.
- [4] Peixiang Zhao, Charu C Aggarwal, and Min Wang. gsketch: on query estimation in graph streams. *Proc. VLDB*, 2011.
- [5] Amit Goyal, Daume, Hal Iii, and Graham Cormode. Sketch algorithms for estimating point queries in nlp. In *Joint Conference on Empirical Methods in Natural Language Processing and Computational Natural Language Learning*, 2012.
- [6] Graham Cormode, Theodore Johnson, Flip Korn, S Muthukrishnan, Oliver Spatscheck, and Divesh Srivastava. Holistic udafs at streaming speeds. In *Proc. ACM SIGMOD*, pages 35–46. ACM, 2004.
- [7] Pratanu Roy, Arijit Khan, and Gustavo Alonso. Augmented sketch: Faster and more accurate stream processing.
- [8] Graham Cormode and S Muthukrishnan. An improved data stream summary: the count-min sketch and its applications. *Journal of Algorithms*, 55(1):58–75, 2005.
- [9] Graham Cormode. Sketch techniques for approximate query processing. *Foundations and Trends in Databases*. NOW publishers, 2011.
- [10] Charu C Aggarwal and S Yu Philip. On classification of high-cardinality data streams. In *SDM*, volume 10, pages 802–813. SIAM, 2010.
- [11] Aiyu Chen, Yu Jin, Jin Cao, and Li Erran Li. Tracking long duration flows in network traffic. In *Proc. IEEE INFOCOM*, 2010.
- [12] Graham Cormode and Minos Garofalakis. Sketching streams through the net: Distributed approximate query tracking. In *Proc. VLDB*, 2005.
- [13] Graham Cormode and Marios Hadjieleftheriou. Finding frequent items in data streams. *Proceedings of the VLDB Endowment*, 1(2):1530–1541, 2008.
- [14] Zaoying Liu, Antonis Manousis, and et al. One sketch to rule them all: Rethinking network flow monitoring with univmon. In *Proc. ACM SIGCOMM*, 2016.
- [15] Dina Thomas, Rajesh Bordawekar, and et al. On efficient query processing of stream counts on the cell processor. In *Proc. IEEE ICDE*, 2009.
- [16] Anna C Gilbert, Martin J Strauss, Joel A Tropp, and Roman Vershynin. One sketch for all: fast algorithms for compressed sensing. In *Proc. ACM STOC*, 2007.
- [17] David Talbot and Miles Osborne. Smoothed bloom filter language models: Tera-scale lms on the cheap. In *EMNLP-CoNLL*, pages 468–476, 2007.
- [18] Benjamin Van Durme and Ashwin Lall. Probabilistic counting with randomized storage. In *IJCAI*, pages 1574–1579, 2009.
- [19] Neoklis Polyzotis, Minos Garofalakis, and Yannis Ioannidis. Approximate xml query answers. In *Proc. ACM SIGMOD*, 2004.
- [20] Joshua Spiegel and Neoklis Polyzotis. Graph-based synopses for relational selectivity estimation. In *Proc. ACM SIGMOD*, 2006.
- [21] Andrea Pietracaprina, Matteo Riondato, Eli Upfal, and Fabio Vandin. Mining top-k frequent itemsets through progressive sampling. *Data Mining and Knowledge Discovery*, 21(2):310–326, 2010.
- [22] Cristian Estan and George Varghese. New directions in traffic measurement and accounting. *ACM SIGCOMM CCR*, 32(4), 2002.
- [23] Moses Charikar, Kevin Chen, and Martin Farach-Colton. Finding frequent items in data streams. In *Automata, Languages and Programming*. Springer, 2002.
- [24] Tong Yang, Lingtong Liu, Yibo Yan, Muhammad Shahzad, Yulong Shen, Xiaoming Li, Bin Cui, and Gaogang Xie. Sf-sketch: A fast, accurate, and memory efficient data structure to store frequencies of data items. In *Proc. IEEE ICDE*, 2017.
- [25] Yang Zhou, Peng Liu, Hao Jin, Tong Yang, and Xiaoming Li. One memory access sketch: a more accurate and faster sketch for per-flow measurement. *IEEE Globecom*, 2017.
- [26] Burton H Bloom. Space/time trade-offs in hash coding with allowable errors. *Communications of the ACM*, 13(7):422–426, 1970.
- [27] Li Fan, Pei Cao, Jussara Almeida, and Andrei Z Broder. Summary cache: a scalable wide-area web cache sharing protocol. *IEEE/ACM ToN*, 2000.
- [28] Saar Cohen and Yossi Matias. Spectral bloom filters. In *Proc. ACM SIGMOD*, pages 241–252, 2003.
- [29] Josep Aguilar-Saborit, Pedro Trancoso, Victor Muntès-Mulero, and Josep-Lluís Larriba-Pey. Dynamic count filters. *ACM SIGMOD Record*, 2006.
- [30] Tong Yang, Alex X. Liu, Muhammad Shahzad, Yuankun Zhong, Qiaobin Fu, Zi Li, Gaogang Xie, and Xiaoming Li. A shifting bloom filter framework for set queries. *Proceedings of the Vldb Endowment*, 9(5):408–419, 2016.
- [31] Tong Yang, Alex X. Liu, Muhammad Shahzad, Dongsheng Yang, Yuankun Zhong, Qiaobin Fu, Zi Li, Gaogang Xie, and Xiaoming Li. A shifting framework for set queries. *IEEE/ACM Transaction on Networking (ToN)*, 2017.
- [32] Yi Lu, Andrea Montanari, Balaji Prabhakar, Sarang Dharmapurikar, and Abdul Kabbani. Counter braids: a novel counter architecture for per-flow measurement. In *Proc. ACM SIGMETRICS*, 2008.
- [33] Cuda toolkit documentation. <http://docs.nvidia.com/cuda/cuda-c-best-practices-guide/index.html#coalesced-access-to-global-memory>.
- [34] Real-life transactional dataset. <http://fimi.ua.ac.be/data/>.
- [35] David MW Powers. Applications and explanations of Zipf’s law. In *Proc. EMNLP-CoNLL*. Association for Computational Linguistics, 1998.
- [36] Alex Rousskov and Duane Wessels. High-performance benchmarking with web polygraph. *Software: Practice and Experience*, 34(2):187–211, 2004.
- [37] Hash website. <http://burtleburtle.net/bob/hash/evahash.html>.